Article

Hydrogen Peroxide Electrogeneration by Gas Diffusion Electrode Modified with Tungsten Oxide Nanoparticles for Degradation of Orange II and Sunset Yellow FCF Azo Dyes

Edson C. Paz,[a,b] Victor S. Pinheiro,[a] Luci R. Aveiro,[a] Fernanda L. Souza,[a] Marcos R. V. Lanza[c,d] and Mauro C. Santos ✴,[a]*

[a]*Laboratório de Eletroquímica e Materiais Nanoestruturados (LEMN),
Centro de Ciências Naturais e Humanas (CCNH), Universidade Federal do ABC (UFABC),
Rua Santa Adélia, 166, 09210-170 Santo André-SP, Brazil*

[b]*Instituto Federal de Educação, Ciência e Tecnologia do Maranhão (IFMA), Campus Açailândia,
R. Projetada, s/n, 65930-000 Açailândia-MA, Brazil*

[c]*Instituto de Química de São Carlos (IQSC), Universidade de São Paulo (USP),
CP 780, 13566-590 São Carlos-SP, Brazil*

[d]*Instituto Nacional de Tecnologias Alternativas para Detecção, Avaliação Toxicológica e
Remoção de Micropoluentes e Radioativos (INCT-DATREM), Instituto de Química,
Universidade Estadual Paulista "Júlio de Mesquita Filho" (Unesp), 14800-900 Araraquara-SP, Brazil*

In this work, the gas diffusion electrode (GDE) cathode of Vulcan XC72 carbon modified with nanoparticles of $WO_{2.72}$ ($WO_{2.72}$ / Vulcan XC72) was used for H_2O_2 electrogeneration and degradation of 350 mL of Orange II (OII) and Sunset Yellow FCF (SY) azo dyes by electro-Fenton (EF) and photoelectro-Fenton (PEF) processes with different Fe^{2+} initial content (1.00, 0.50 and 0.25 mmol L^{-1}). The $WO_{2.72}$ / Vulcan XC72 GDE electrolyzed approximately 3 times more H_2O_2 than the Vulcan XC72 GDE. Decolorizations and mineralizations of the dye solutions were more efficient at higher concentrations of Fe^{2+}. The decolorization decay showed pseudo-first-order kinetics. The most promising decolorization results obtained at processes of $WO_{2.72}$ / Vulcan XC72 cathode combined with Pt anode (100% color removal of OII and SY at 30 and 20 min of electrolysis with 1.00 mmol L^{-1} Fe^{2+}, respectively). The best mineralization achieved in trials of $WO_{2.72}$ / Vulcan XC72 cathode combined with boron-doped diamond (BDD) anode (82% total organic carbon (TOC) removal of OII by PEF / 1.00 after 3 h and 90% TOC removal of SY by PEF / 0.50 after 4 h). It was found that SY decolorization was faster and mineralization showed a similar yield independent of oxidized dye.

Keywords: $WO_{2.72}$ / Vulcan XC72, H_2O_2 electrogeneration, decolorization, mineralization, azo dyes

Introduction

The discharge of large volumes of azo dye industrial effluents into water bodies is a concerning practice because it can generate serious environmental and health problems;[1] such highly colored dyes are a dramatic source of aesthetic pollution,[2] as well as being toxic, carcinogenic[3,4] and mutagenic.[5] Azo dyes are characterized by one or more –N=N– bonds,[3,4] usually conjugated with benzene and/or naphthalene systems.[6] Among different types of dyes, azo dyes are more versatile and represent approximately 70%

of the world's dye production.[7,8] Orange II (OII) (Figure 1a) and Sunset Yellow FCF (SY) (Figure 1b) were used as model azo dyes. OII is very stable and widely used in the textile, food and cosmetic industries.[2,9] SY is extensively used in food, pharmaceuticals and cosmetic products.[4,10,11]

Therefore, the removal of color from aqueous effluents is of remarkable environmental and health importance.[5] Recently, electrochemical advanced oxidation processes (EAOPs) are promising alternatives to conventional methods.[12,13] These processes can lead to a complete mineralization (transformation into CO_2, H_2O and inorganic ions) of persistent organic pollutants in aqueous systems via the *in situ* generation of reactive oxygen species (ROS),
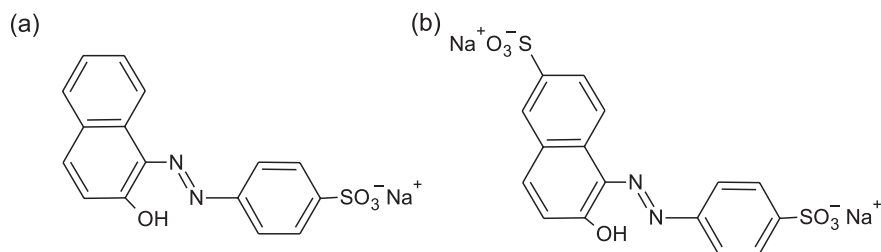
*e-mail: mauro.santos@ufabc.edu.br

(a)

(b)

Figure 1. Molecular structure of (a) OII and (b) SY.[6,8]

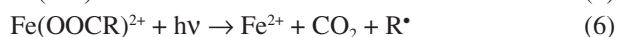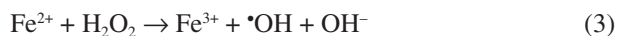such as hydroxyl radicals ($^\bullet$OH), a powerful oxidizing agent.[5,12,14]

Hydroxyl radicals can be produced directly by anodic oxidation (AO) of water (equation 1).[5,15] When active anodes such as Pt, IrO_2 and RuO_2 are employed, the M($^\bullet$OH) radicals have a weaker oxidizing ability because they are chemisorbed.[1] In contrast, non-active anodes, like PbO_2 and boron-doped diamond (BDD), favor the electrochemical incineration of organics because they generate physiosorbed M($^\bullet$OH) with very weak M–$^\bullet$OH interactions, resulting in a greater O_2-overpotential and a quicker destruction of organics.[1,14]

$$M + H_2O \rightarrow M(^\bullet OH) + H^+ + e^- \qquad (1)$$
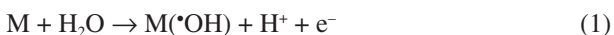
Hydroxyl radicals can also be produced indirectly via electrogenerated Fenton's reagent (H_2O_2 / Fe^{2+}).[5,6,16] In this case, the H_2O_2 is produced by the oxygen reduction reaction (ORR) two-electron pathway in carbonaceous cathodes (equation 2).[15,17,18] The H_2O_2 can be produced by gas diffusion electrode (GDE) cathodes, which are advantageous due to the large contact areas among the cathode, oxygen and water.[19]

$$O_2 + 2H^+ + 2e^- \rightarrow H_2O_2 \qquad (2)$$

Most recently, there have been increased efforts in developing EAOPs based on *in situ* hydrogen peroxide production, such as the electro-Fenton (EF) and photoelectro-Fenton (PEF) processes.[20,21] In EF, the electrogenerated H_2O_2 reacts with externally added Fe^{2+} ions to produce hydroxyl radicals and Fe^{3+} ions, according to Fenton's reaction (equation 3).[5,15,22] The generated Fe^{3+} ions are reduced to Fe^{2+} at the cathode (equation 4).[16,21] EF can be improved by the incidence of UV light into the reaction medium. This process is called PEF, in which the radiation facilitates the degradation of organic compounds due to the faster regeneration of Fe^{2+} and increased $^\bullet$OH production induced by the photoreaction of $Fe(OH)^{2+}$ species (equation 5) and the photolysis of complexes of Fe^{III}-carboxylate (equation 6),[20,23] in which carbon-centered radicals ($R^\bullet$) are also formed.[24]

$$Fe^{2+} + H_2O_2 \rightarrow Fe^{3+} + {}^\bullet OH + OH^- \qquad (3)$$
$$Fe^{3+} + e^- \rightarrow Fe^{2+} \qquad (4)$$
$$Fe(OH)^{2+} + h\nu \rightarrow Fe^{2+} + {}^\bullet OH \qquad (5)$$
$$Fe(OOCR)^{2+} + h\nu \rightarrow Fe^{2+} + CO_2 + R^\bullet \qquad (6)$$

At this point, our group has worked to develop new electrocatalytic materials with high performance in the peroxide electrogeneration for environmental applications. In our previous work, we demonstrated the physical and electrocatalyst properties of $WO_{2.72}$ supported on Vulcan XC72 carbon.[25] The material showed high performance in H_2O_2 electrogeneration, with good current efficiency (CE) and lower energy consumption (EC).[25] For this reason, in this work, this new material ($WO_{2.72}$ / Vulcan XC72) was used to produce a GDE cathode. This cathode was combined with the Pt and BDD anodes for decolorization and mineralization of OII and SY azo dyes by EF and PEF processes. The effect of the initial concentrations of Fe^{2+} ions (0.25, 0.50 and 1.00 mmol L^{-1}) was studied with the intention of elucidating how the mediated electrolytic process affects dye oxidation. All these trials had the main objective of determining the best parameters for application of the $WO_{2.72}$ / Vulcan XC72 cathode in the degradation of the dyes. In addition, to evaluate the influence of the structure of the dyes in the oxidation processes by Fenton's reaction.

Experimental

Preparation of GDE electrode

First, the $WO_{2.72}$ / Vulcan XC72 electrocatalyst was prepared. The $WO_{2.72}$ nanoparticles (NPs) anchored on Vulcan XC72 carbon (Cabot Corporation) without any previous treatment were prepared by the modified polymeric precursor method (PPM) at the mass ratio of 1:100 (W:C).[25-27] All reagents used were purchased from Sigma-Aldrich (St. Louis, USA). The GDE cathode was prepared by the hot pressing procedure using $WO_{2.72}$ / Vulcan XC72 and Vulcan XC72 with 20% (m/m) of a 60% aqueous dispersion from Sigma-Aldrich. A sintered 3-mm-thick GDE was obtained after 2 h at 290 °C, under load of 18 MPa, as proposed by other works.[25,28,29]

Physical characterization

Physical characterizations were performed by X-ray diffraction (XRD), X-ray photoelectron spectroscopy (XPS), transmission electron microscopy (TEM), energy dispersive spectroscopy (EDS) and contact angle measurements.

XRD was conducted on a Rigaku-MiniFlex X-ray diffractometer with a continuous Cu Kα radiation source (2° min^{-1}) at intervals of $20-60^o$.[25] XPS spectra were measured at a pressure of less than 10^{-7} Pa using a commercial spectrometer (UNI-SPECS UHV). The Al Kα line was used (hν = 1486.6 eV), and the analyzer pass energy was set to 10 eV. The inelastic background of the W 4f, O 1s and C 1s high-resolution core-level spectra were subtracted using Shirley's method. The spectra were fitted without placing constraints using multiple Voigt profiles in the CasaXPS software.[30] TEM images were collected with a JEOL JEM-2100 electron transmission microscope operating at 200 kV. The samples for the TEM studies were prepared by placing nanodispersion droplets on a carbon-coated copper grid and evaporating the solvent at room temperature.[25,31] The EDS analyses were performed using an EDS chemical microanalysis module coupled to a JEOL JSM-6010LA compact sweep electron microscope.[25] Contact angle was determined on a goniometer (GBX Digidrop) by dropping a water droplet (5 μL) onto the electrocatalyst surface.[25] Windrop++ software was used.

Electrochemical measurements

Hydrogen peroxide electrogeneration in GDE cathode

H_2O_2 was generated by electrolysis performed with a 3.0 cm^2 exposed area GDE cathode supplied with O_2 at 0.2 bar. An undivided cell was used containing 350 mL aqueous electrolyte (0.1 mol L^{-1} H_2SO_4 and 0.1 mol L^{-1} K_2SO_4 at 20 ^{o}C and pH 3.0), with Ag / AgCl (analyzer) and 7.5 cm^2 Pt electrodes as the reference and auxiliary electrodes, respectively. The distance between cathode and anode was 1.0 cm.

Decolorization and mineralization of OII and SY solutions

Comparative degradations by EF and PEF were carried out with 350 mL of 0.260 mmol L^{-1} (50 mg L^{-1} of total organic carbon (TOC)) OII (Sigma-Aldrich, St. Louis, USA) or SY (Sigma-Aldrich, St. Louis, USA) in 0.1 mol L^{-1} K_2SO_4 at 20 ^{o}C. An undivided cell was used with a 7.5 cm^2 BDD (thin-film from NeoCoat; substrate: polycrystalline Si, dopant amount: 5000 ppm) or Pt anode and a 3.0 cm^2 WO$_{2.72}$ / Vulcan XC72 GDE cathode supplied with O_2 at 0.2 bar. The distance between the cathode and anode

was 1.0 cm. Ag / AgCl was used as the reference electrode. All processes evaluated were conducted potentiostatically at –1.9 V *vs.* Ag / AgCl. The EF and PEF trials were performed at pH 3.0 and with the addition of 0.25, 0.50 or 1.00 mmol L^{-1} Fe^{2+}. The photodegradation was carried out using a mercury UV lamp of λ_{max} = 254 nm immersed in the solution, positioned at 2 cm from the GDE cathode.

Analytical procedures

The hydrogen peroxide was quantified via UV-Vis by reacting 0.5 mL of the electrolyte containing H_2O_2 with 4 mL of a solution containing 2.4×10^{-3} mol L^{-1} $(NH_4)_6Mo_7O_{24}$ and 0.5 mol L^{-1} H_2SO_4, with the absorption measured at 350 nm.[25,29] The H_2O_2 concentration was determined from a previously constructed analytical curve using a Varian Cary 50 Scan UV-Vis spectrophotometer.[25] The limit of detection (LOD) was 34.6 mg L^{-1}.

The decolorization of OII and SY solutions was determined by the decrease of their absorbance (A) at the maximum visible wavelength of λ_{max} = 484 and 482 nm, respectively. This procedure was conducted employing a UV-Vis spectrophotometer (Varian Cary 50 Scan). Dye solution aliquots of 0.5 mL were diluted in 4 mL electrolyte (0.1 mol L^{-1} H_2SO_4 and 0.1 mol L^{-1} K_2SO_4) and analyzed between 200 and 800 nm at 20 ^{o}C.

All samples extracted from electrolyzed solutions were treated with sodium sulfite to stop the mineralization process and filtered through 0.45 μm polytetrafluoroethylene (PTFE) filters from Analítica before analysis. The TOC concentration was monitored using a TOC-V CPN Shimadzu analyzer.

Results and Discussion

Physical characterization

The results of the physical characterization of the WO$_{2.72}$ / Vulcan XC72 electrocatalyst were presented in detail in the article published previously by our group.[25] Briefly, XRD analysis showed the presence of the monoclinic crystalline phase WO$_{2.72}$ (W$_{18}$O$_{49}$).[25] The XPS analysis showed that the material modified with the WO$_{2.72}$ nanoparticles presented a high content of oxygenated acidic groups.[25] The micrographs obtained by TEM showed the dispersion and shape of the nanometer structure of the WO$_{2.72}$ phase anchored on Vulcan XC72 carbon. The EDS analysis presented the W:C estimated content to be approximately 0.8% (m/m), close to the nominal value of 1.0% (m/m).[25] The contact angle values showed that the WO$_{2.72}$ / Vulcan XC72 material is more hydrophilic than pure Vulcan XC72.[25]

Hydrogen peroxide electrogeneration in GDE cathode

The H_2O_2 electrogeneration was performed using unmodified Vulcan XC72 and $WO_{2.72}$ / Vulcan XC72 GDEs over a wide range of applied cathodic potential (–0.7 to –2.5 V *vs.* Ag / AgCl). Figure 2 shows the H_2O_2 electrogeneration as a function of electrolysis time for different values of applied potentials obtained with unmodified Vulcan XC72 and modified Vulcan XC72 ($WO_{2.72}$ / Vulcan XC72) GDEs. As can be observed, an increase in cathodic applied potential caused an improvement in the H_2O_2 electrogeneration in both GDEs studied. This was a surprise, as there is usually a reduction of H_2O_2 generation when high cathodic potentials are applied during electrolysis. Such behavior of the studied GDEs can be justified by the attenuation or absence of parallel reactions, such as the reduction of H_2O_2 to H_2O, H_2 evolution and the ORR four-electron pathway, which can occur in electrolysis at higher applied potentials.[32,33]

Table 1 shows the accumulated H_2O_2 from the Vulcan XC72 and $WO_{2.72}$ / Vulcan XC72 GDEs after 120 min of electrolysis. The $WO_{2.72}$ / Vulcan XC72 GDE accumulated more H_2O_2 than the Vulcan XC72 GDE at all studied potentials (1.5, 2.9, 2.8 and 2.8 times higher at –0.7, –1.3, –1.9 and –2.5 V *vs.* Ag / AgCl, respectively). These results show how much the modification with the $WO_{2.72}$ nanoparticles improved the electrocatalytic activity of Vulcan XC72 carbon for H_2O_2 electrogeneration and, consequently, for application in the degradation of organic pollutants by EF processes and derivatives. We attributed the improved electrocatalytic to the higher hydrophilicity of $WO_{2.72}$ / Vulcan XC72 due to the increase of acid oxygen groups resulting from the modification of Vulcan XC72 carbon with the nanoparticles of $WO_{2.72}$.[25] Hydrophilic

materials favor the adsorption of O_2 according to the Pauling model.[18,25] This allows the ORR by two-electron pathway resulting in the formation of H_2O_2.[18,25]

Table 1. Accumulated H_2O_2 by Vulcan XC72 and $WO_{2.72}$ / Vulcan XC72 GDEs at different potentials after 120 min of electrolysis

E / V *vs.* Ag / AgCl	$[H_2O_2]$ / (mg L^{-1})	
	Vulcan XC72	$WO_{2.72}$ / Vulcan XC72
–0.7	218.9	325.0
–1.3	259.4	755.0
–1.9	354.7	976.7
–2.5	407.4	1124.9

Additionally, it is important to know the EC and the CE for the H_2O_2 electrogeneration. The EC (in kWh kg^{-1}) and the CE (in %) for the H_2O_2 electrogeneration were determined from equations 7[34] and 8,[35] respectively.

$$EC = \frac{I\,E_{cell}\,t}{1000m} \tag{7}$$

$$CE = \frac{z\,F\,[H_2O_2]\,V}{M_{H_2O_2}\,I\,t_s} \tag{8}$$

where I represents the current (A), E_{cell} is the cell potential (V), t is the time (h), m is the mass of hydrogen peroxide formed (kg), z is the number of electrons transferred for the oxygen reduction to H_2O_2, F is the Faraday constant (96,485 C mol^{-1}), $[H_2O_2]$ is the concentration of H_2O_2 (g L^{-1}), V is the solution volume (L), $M_{H_2O_2}$ is the molar mass of H_2O_2 (34.01 g mol^{-1}), and t_s is the electrolysis time (s).

The EC and the CE for the H_2O_2 electrogeneration for 120 min by Vulcan XC72 and $WO_{2.72}$ /
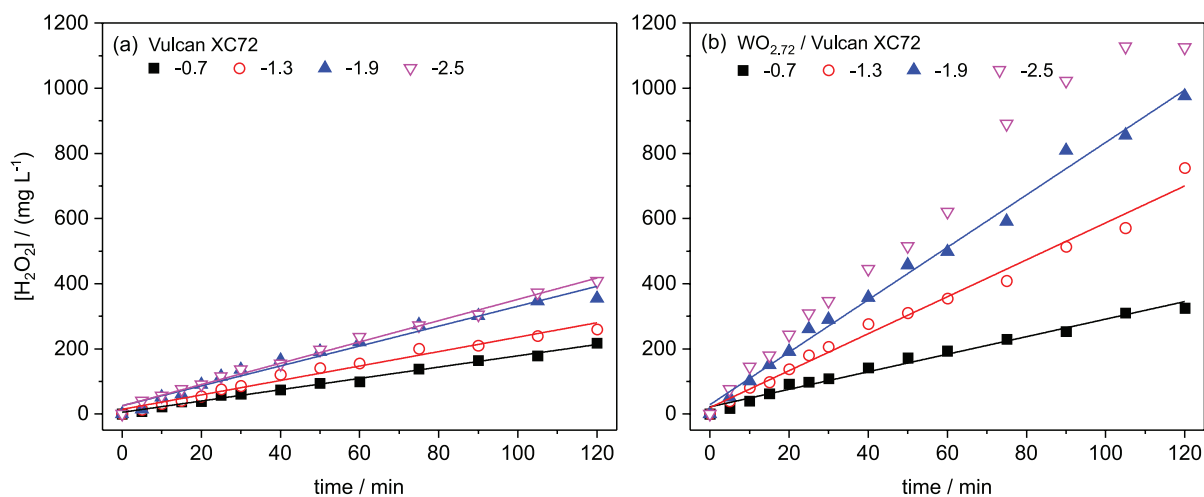

Figure 2. H_2O_2 electrogeneration at different applied potentials as a function of the electrolysis time for the GDEs of (a) Vulcan XC72 and (b) $WO_{2.72}$ / Vulcan XC72.

Vulcan XC72 GDEs are shown in Figure 3. As seen, the $WO_{2.72}$ / Vulcan XC72 GDE consumed less power than the Vulcan XC72 GDE (1.7, 2.6, 3.1 and 3.1 times lower at –0.7, –1.3, –1.9 and –2.5 V *vs.* Ag / AgCl, respectively). In addition, the EC increased in both GDEs due to the increase of the applied potential. The CE of $WO_{2.72}$ / Vulcan XC72 GDE was superior to the CE of Vulcan XC72 GDE at all potentials. The values were 1.6, 2.7, 3.0 and 2.9 times higher at –0.7, –1.3, –1.9 and –2.5 V *vs.* Ag / AgCl, respectively. Contrary to the EC, CE decreased as the applied potential was increased, from 38.1 and 62.7% at –0.7 V to 15.3 and 44.8% at –2.5 V for modified and unmodified Vulcan GDE, respectively. Higher EC and lower CE for the H_2O_2 electrogeneration at higher potentials can be justified by parasitic reactions such as H_2O_2 reduction on the cathode to H_2O, its oxidation in the anode and H_2 evolution reactions.[33] In addition, other works have demonstrated that the decomposition of H_2O_2 is favored in smaller volumes,[25,35] and, at higher potentials, the process can be controlled by mass transfer from dissolved oxygen.[25,35]
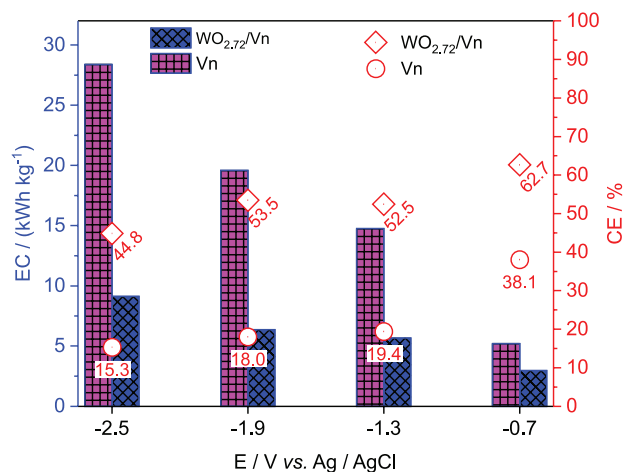

Figure 3. EC and CE for H_2O_2 electrogeneration of Vulcan XC72 and $WO_{2.72}$ / Vulcan XC72 GDEs at different potentials after 120 min of electrolysis.

The results of H_2O_2 electrogeneration show that the $WO_{2.72}$ / Vulcan XC72 GDE is a very promising cathodic material, particularly when it is compared to other cathodic materials published in the literature recently, as seen in Table 2.[34,36-38]

Decolorization of OII and SY solutions

Treatments of 350 mL solutions containing 50 mg L^{-1} of TOC of OII (91.2 mg L^{-1}) or SY (117.8 mg L^{-1}) in the presence of 0.1 mol L^{-1} K_2SO_4 at pH 3.0 were carried out at –1.9 V *vs.* Ag / AgCl (3 mol L^{-1}) and 20 °C. Figure 4

Table 2. Comparisons of H_2O_2 generation rate between this work and representative published data obtained from cathode materials[36]

Cathode material	H_2O_2 generation rate / (mg L^{-1} h^{-1} cm^{-2})	Reference or applied potential
PPy / lig-GF	10.1	[36]
GF-Co	13.9	[37]
NCNT / NF / CNT	42.2	[38]
CoPc / Px 5%	64.9	[34]
$WO_{2.72}$ / Vn	54.2	–0.7 V *vs.* Ag / AgCl[a]
$WO_{2.72}$ / Vn	125.8	–1.3 V *vs.* Ag / AgCl[a]
$WO_{2.72}$ / Vn	162.8	–1.9 V *vs.* Ag / AgCl[a]
$WO_{2.72}$ / Vn	187.5	–2.5 V *vs.* Ag / AgCl[a]

[a]Applied potential during the electrolysis of this work. lig-GF: lignin-graphite felt; NCNT / NF / CNT: N-doped multi-walled carbon nanotubes / nickel foam / multi-walled carbon nanotubes; CoPc / Px: cobalt(II) phthalocyanine / Printex 6L carbon; Vn: Vulcan XC72.

shows percentage of OII and SY removal by EF and PEF processes as a function of time for different values of Fe^{2+} initial concentrations equal to 1.00, 0.50 and 0.25 mmol L^{-1}, employing a $WO_{2.72}$ / Vulcan XC72 GDE cathode and Pt or BDD as the anode. The decolorization efficiency for EF and PEF processes was calculated from equation 9:[22]

$$\% \text{ Color removal} = \frac{A_0 - A_t}{A_0} \times 100 \qquad (9)$$

where A_0 and A_t are the absorbance at initial time and time t, respectively, at λ_{max} = 484 and 482 nm for OII and SY, respectively.[8,22,25]

For the processes using Pt as anode, 100% of decolorization was attained in approximately 30, 40 and 105 min for OII and 20, 40 and 90 min for SY at 1.00, 0.50 and 0.25 mmol L^{-1} Fe^{2+}, respectively (Figure 4). In processes with BDD, the complete decolorization was attained after approximately 60 min of electrolysis for OII (Figure 4a) and after 30, 60 and 75 min, 98-100% of the SY had been removed at 1.00, 0.50 and 0.25 mmol L^{-1} Fe^{2+}, respectively (Figure 4b). The decolorizations increased at higher Fe^{2+} concentrations at all processes because of the higher amount of hydroxyl radicals generated according to Fenton's reaction (equation 3).[1,5,15] A similar pattern of color removal was found for OII e SY using Pt and BDD anodes. However, the decolorizations with 1.00 and 0.50 mmol L^{-1} Fe^{2+} with the Pt anode were faster than processes with the BDD anode. These results can be justified by the faster oxidation of Fe^{2+} to Fe^{3+} on the surface of the anode of BDD (equation 10) and by the consumption of Fe^{2+} that reacts with the $S_2O_8^{2-}$ formed on the surface of the BDD (equation 11).[19,39] Such reactions
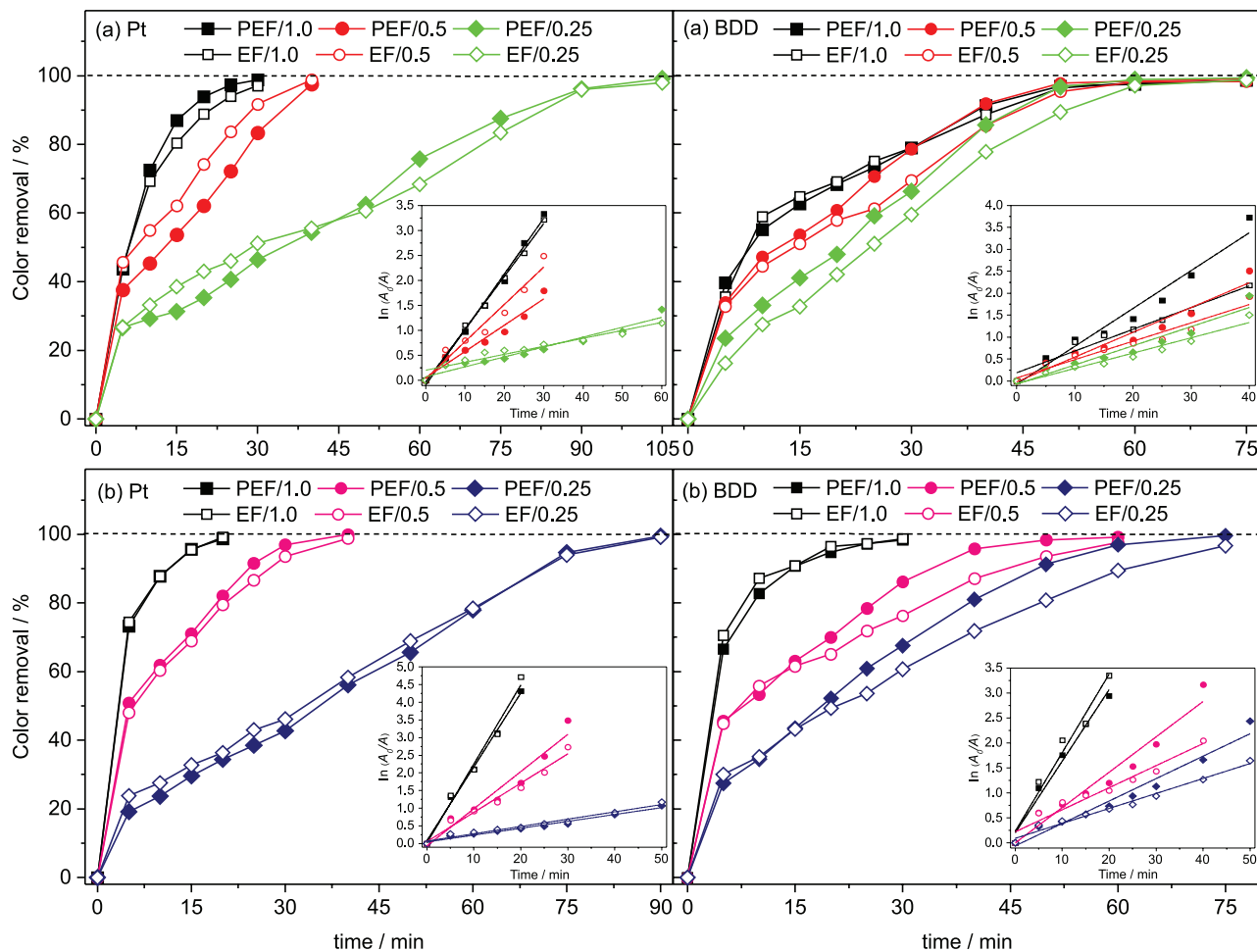
Figure 4. Decolorization of (a) OII and (b) SY solutions as a function of time by EF and PEF processes at different initial concentrations of Fe^{2+} (0.25, 0.50 and 1.00 mmol L^{-1}) with Pt and BDD anodes. The inset panel presents the corresponding pseudo-first-order kinetic analysis.

reduce the concentration of $^\bullet OH$ produced by the Fenton reaction (equation 3).[5,19,39]

$$Fe^{2+} \rightarrow Fe^{3+} + e^- \tag{10}$$
$$S_2O_8^{2-} + 2Fe^{2+} \rightarrow 2SO_4^{2-} + 2Fe^{3+} \tag{11}$$
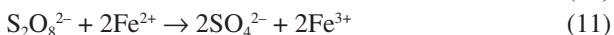
The determination of decolorization EC is an important parameter because it provides information for selecting the best cost-benefit process. The decolorization EC *per* volume unit (in kWh m^{-3}) for the trials made with 350 mL solution were obtained from equation 12:[8]

$$EC = \frac{E_{cell} \, I \, t}{V_s} \tag{12}$$

where E_{cell} is the average potential difference of the cell (V), I is the applied current (A), t is the electrolysis time (h) and V_s is the solution volume (L).

Figure 5 shows the EC of decolorization of OII and SY. It can be observed that the EC in the processes using the Pt anode was inversely proportional to the Fe^{2+} concentration. This observation can be explained taking into account the effect on conductivity of the production of protons and hydroxyl ions caused by Fenton's reactions, which lead to faster decolorization. The decolorization with the BDD anode showed similar EC in the most processes, which was higher than the EC of the decolorization with Pt anodes. This tendency may be attributed to the fact that parasite reactions are consuming hydroxyl radicals and other significant oxidants, limiting the action of the radicals on the dye oxidation. In this way, decolorization with Pt was faster, and smaller potential differences between the electrodes are provided to the Pt / GDE cell at the same current density.[22] From these results, it can be inferred that the decolorizations of OII and SY with Pt anode in 1.00 mmol L^{-1} Fe^{2+} presented the best cost-benefit.

The kinetics of decolorization of OII and SY solutions can be described as a pseudo-first-order reaction by:[8,40]
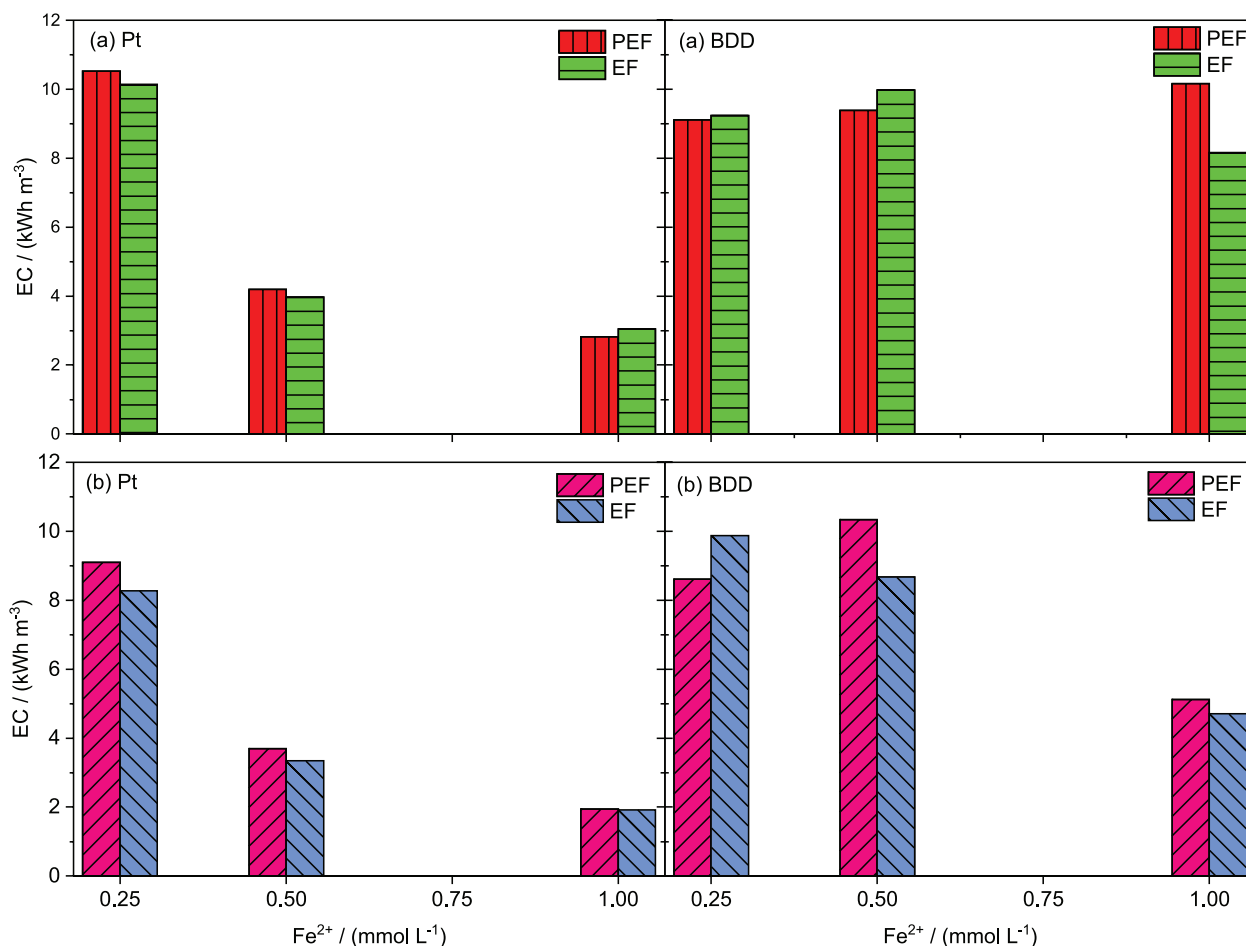
$$A = A_0 e^{-k_1 t} \tag{13}$$

Figure 5. EC at the decolorization of (a) OII and (b) SY solution by EF and PEF processes with different initial concentrations of Fe^{2+} (0.25, 0.50 and 1.00 mmol L^{-1}) with Pt and BDD anodes.

$$\ln(A_0 / A) = k_1 t \qquad (14)$$

where A_0 and A_t are the absorbance at initial time and time t, respectively, at $\lambda_{max} = 484\ 482$ nm for OII and SY, respectively; k_1 (min^{-1}) is the pseudo-first-order kinetic constant and t (min) is the decolorization time.

The absorbance decays were well-fitted to a pseudo-first-order kinetic equation, as seen in the inset of Figure 4. This suggests the constant production of oxidant •OH in the systems that accelerates the oxidation rate of both dyes.[8] Table 3 shows the pseudo-first-order kinetic constants (k_1) and the corresponding squares of the correlation coefficients (R^2) for the decolorization of OII and SY. The k_1 values of OII and SY increased by increasing Fe^{2+} concentrations. The k_1 increased from 0.021 to 0.223 min^{-1} when the Fe^{2+} concentration increased from 0.25 to 1.00 mmol L^{-1} for the decolorization of SY by EF with Pt, for example. The decolorization of OII and SY with Pt is very low at the lower Fe^{2+} concentration. This indicate that this Fe^{2+} content is insufficient to propagate Fenton's reaction, and thus, it diminishes the oxidation

efficiency of the dye. In addition, the k_1 values were higher in the SY decolorizations compared to OII decolorization under similar conditions.

Considering the decolorizations of OII and SY dyes under same conditions (anode and Fe^{2+} initial concentration), it was observed that: (*i*) the EF and PEF processes showed similar decolorization efficiency, indicating that the color removal process was controlled mainly by Fenton's reaction (equation 3)[1] and direct anodic oxidation (equation 1);[5] and (*ii*) the color removal of SY was faster than OII. We believe that to be due to the chemical structure of SY because it contains two sulfonic groups (Figure 1), which are negative and repel each other, leaving the azo group (–N=N–) more exposed and susceptible to the attack of hydroxyl radicals.

Mineralization of OII and SY solutions

Solutions of 350 mL of the OII or SY dye were submitted to mineralization by EF and PEF processes with different Fe^{2+} initial concentrations (0.25, 0.50 and 1.00 mmol L^{-1}). The GDE cathode of $WO_{2.72}$ / Vulcan XC72

Table 3. Pseudo-first-order kinetic constants (k_1) and corresponding square of the correlation coefficient (R^2) for decolorizations of OII and SY at $\lambda_{max} = 484$ and 482 nm, respectively, by EF and PEF processes with different initial concentrations of Fe^{2+} with Pt and BDD anodes

Dye	Process	Fe^{2+} / (mmol L^{-1})	Anode			
			Pt		BDD	
			k_1 / min^{-1}	R^2	k_1 / min^{-1}	R^2
Orange II	EF	1.00	0.106	0.996	0.050	0.961
		0.50	0.074	0.952	0.042	0.942
		0.25	0.016	0.917	0.035	0.951
	PEF	1.00	0.111	0.993	0.086	0.961
		0.50	0.053	0.949	0.056	0.948
		0.25	0.019	0.943	0.043	0.928
Sunset Yellow FCF	EF	1.00	0.223	0.979	0.157	0.958
		0.50	0.083	0.969	0.044	0.944
		0.25	0.021	0.966	0.030	0.978
	PEF	1.00	0.209	0.993	0.143	0.974
		0.50	0.105	0.940	0.071	0.945
		0.25	0.019	0.975	0.049	0.962

BDD: boron-doped diamond; k_1: pseudo-first-order kinetic constant; R^2: square of the correlation coefficient; EF: electro-Fenton; PEF: photoelectro-Fenton.

was combined with Pt or BDD anode. Figure 6 show results of mineralization of OII and SY as a function of time. In general, (*i*) the processes with the highest Fe^{2+} initial concentration obtained higher mineralization rates of the dyes employing Pt anode and, (*ii*) in the experiments with BDD anode, the highest TOC removals occurred in the processes at 0.5 mol L^{-1} Fe^{2+}.

Comparing the mineralizations of the OII and SY under the same conditions (i.e., same anode and initial Fe^{2+} concentrations), the mineralization efficiency of the PEF process was superior to the EF process (Figure 6). This behavior was expected as the incidence of UV radiation in the system allows the photolytic reactions (equations 5 and 6), which contribute to higher Fe^{2+} availability and degradation of Fe^{III}-carboxylate complexes, making mineralization more efficient.[20,23] In addition, the mineralization of these dyes with BDD anode was more efficient than with Pt anode. BDD($\cdot$OH) has a higher oxidation/mineralization power for organic compounds than Pt($\cdot$OH), because BDD has O_2 evolution overpotential and its hydroxyl radicals ($\cdot$OH) are physisorbed at the anode surface.[12,14] Pt has smaller O_2 evolution overpotential and its hydroxyl radicals are chemisorbed on the Pt surface.[14]

We also observed a sudden decrease in the mineralization rate of OII and SY dyes with Pt by EF / 1.00, EF / 0.50 and EF / 0.25 after 60, 60 and 120 min of electrolysis, respectively (Figure 6). This can be explained by the formation of recalcitrant intermediates, which cannot be degraded by the reactions of equations 1 and 3.[8,12,14]

A decrease in the mineralization rate of PEF processes with Pt at longer electrolysis time was also seen, but it was mild and after higher TOC removal (Figure 6). The action of UV radiation allows the photolytic reactions (equations 5 and 6) to produce more hydroxyl radicals that have oxidative action on stable intermediates, which is not possible solely by EF process.[1,8] Then, with the exception of OII mineralization by PEF / 1.00 and PEF / 0.50 processes, the other processes with Pt showed a stagnation of TOC removal after a certain time. This means that if the electrolysis time were extended, the total mineralization of the dyes OII and SY would not be achieved. In contrast, when BDD was used, almost complete mineralization was attained at 240 min, showing a clear trend for total decay even for SY by PEF / 1.00 and EF / 1.00, which showed slower decay (Figure 6).

From TOC decay, the EC *per* unit TOC mass (EC_{TOC}, in kWh (kg TOC)$^{-1}$)[8] and the mineralization CE (MCE, in %) were obtained from equations 15 and 16, respectively:[22]

$$EC_{TOC} = \frac{1000 E_{cell} \, I \, t}{V_s \Delta(TOC)_{exp}} \qquad (15)$$

$$MCE(\%) = \frac{n \, F \, V_s \Delta(TOC)_{exp}}{4.32 \times 10^7 \, m \, I \, t} \times 100 \qquad (16)$$

where 1000 is a conversion factor (mg g^{-1}), E_{cell} is the average potential difference of the cell (V), I is the applied current (A), t is the electrolysis time (h), V_s is the solution volume
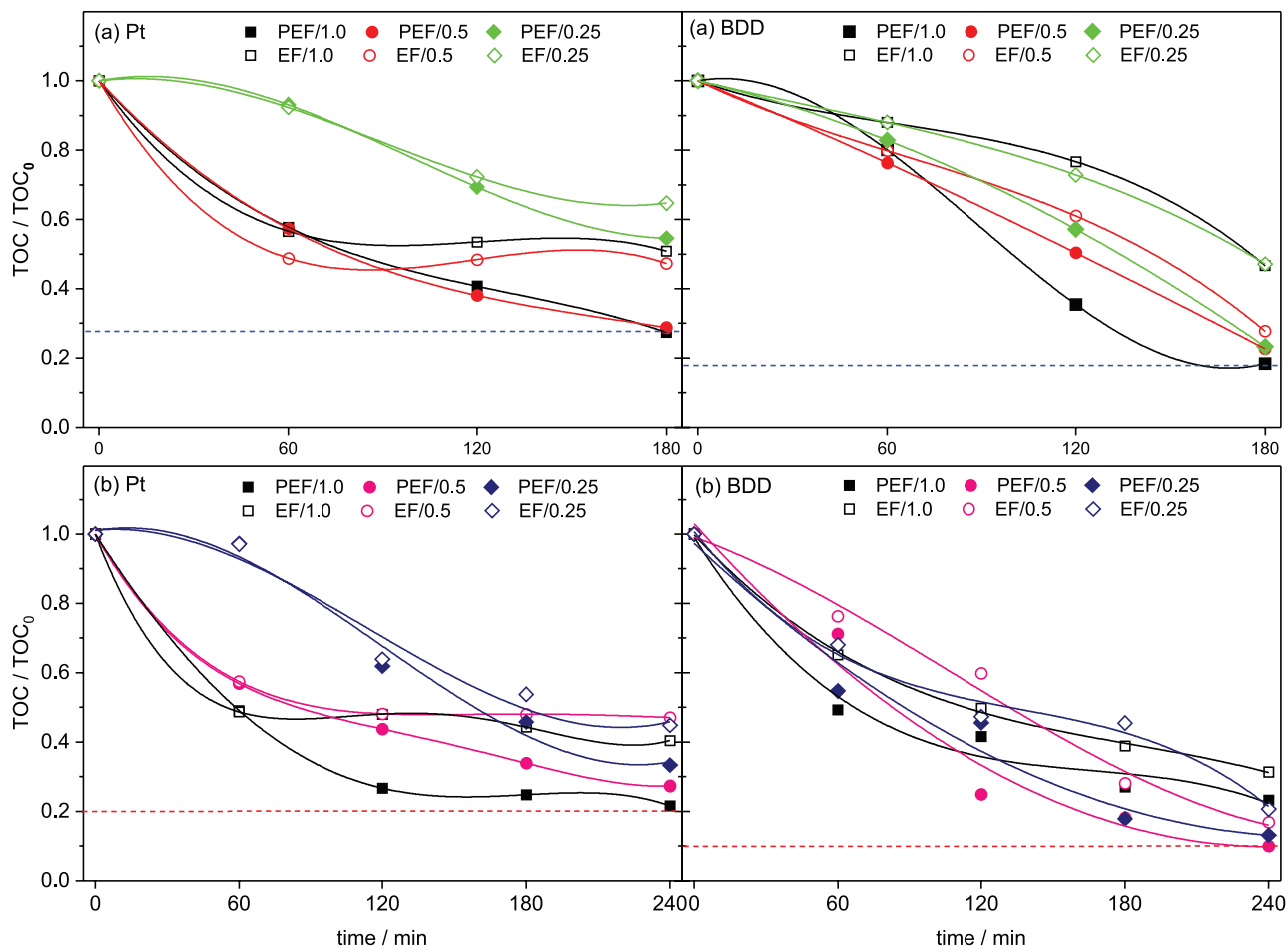
Figure 6. Normalized TOC removal of (a) OII and (b) SY solutions as a function of time by EF and PEF processes at different initial concentrations of Fe^{2+} (0.25, 0.50 and 1.00 mmol L^{-1}) with Pt and BDD anodes.

(L), $\Delta(TOC)_{exp}$ is the experimental TOC decay (mg L^{-1}), n is the theoretical number of electrons consumed *per* dye molecule for overall mineralization, F is the Faraday constant (96,487 C mol^{-1}), 4.32×10^7 is a conversion factor to homogenize units (3600 s $h^{-1} \times 12,000$ mg mol^{-1}) and m is the number of carbon atoms of the azo dye.

Studies have shown that the mineralization of N present in azo dyes by EF processes can generate NO_3^-, NO_2^- and NH_4^+.[22,41-45] Normally, NO_3^- is formed in the greatest quantity.[22,41-45] Thus, we consider the mineralization of OII and SY as their conversion into CO_2 with the release of NO_3^- and SO_4^{2-} as major inorganic ions, according to equations 17 and 18, respectively. Then, the theoretical number of electrons consumed *per* dye molecule (n) for overall mineralization is 84.[22,41]
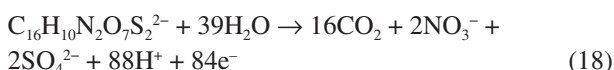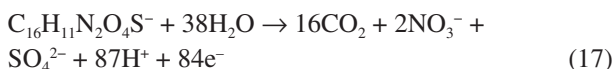
$$C_{16}H_{11}N_2O_4S^- + 38H_2O \rightarrow 16CO_2 + 2NO_3^- + SO_4^{2-} + 87H^+ + 84e^- \tag{17}$$

$$C_{16}H_{10}N_2O_7S_2^{2-} + 39H_2O \rightarrow 16CO_2 + 2NO_3^- + 2SO_4^{2-} + 88H^+ + 84e^- \tag{18}$$

Table 4 shows values of EC and MCE of combustions of OII and SY by EF and PEF processes with different initial concentration of Fe^{2+} using $WO_{2.72}$ / Vulcan XC72 GDE cathode and Pt or BDD anode. In general, the incinerations of OII and SY presented increasing EC and decreasing MCE at longer electrolysis times for both EF and PEF processes. This can be explained since in the long time of electrolysis, there was a reduction of organic matter available for oxidation and the formation of more recalcitrant byproducts, probably oxidized more slowly by Pt(•OH) or BDD(•OH), limited by their transport towards anode surface.[7]

Incinerations of OII and SY with Pt anode at higher Fe^{2+} contents show lower EC and higher mineralization current efficiencies. This indicates the role of the Fe^{2+} concentration and H_2O_2 electrogenerated in the GDE cathode, since the higher mineralization efficiency was observed in the processes with higher concentrations of Fe^{2+} due to the higher amount of •OH produced by the Fenton reaction (equation 3).[5,15]

In the processes with BDD anode, the mineralizations at lower concentrations of Fe^{2+}, especially at 0.50 mmol L^{-1}

Table 4. Energy consumption and mineralization current efficiency for EF and PEF combustions of OII and SY at different initial concentrations of Fe^{2+} and different anodes

Dye	Anode	Process	time / min	EC / (kWh per kg TOC) Fe^{2+} / (mmol L^{-1})			MCE / % Fe^{2+} / (mmol L^{-1})		
				1.00	0.50	0.25	1.00	0.50	0.25
Orange II	Pt	EF	60	279.7	279.4	1775.8	27.7	27.6	4.3
			120	559.3	595.5	1042.1	14.8	13.9	7.7
			180	850.3	936.8	1317.3	10.4	9.5	6.6
		PEF	60	264.9	354.4	1799.5	29.9	22.4	4.1
			120	393.5	528.4	886.4	21.0	16.3	9.1
			180	529.4	730.9	965.4	17.2	12.5	9.0
	BDD	EF	60	1089.2	855.3	1271.6	7.4	11.0	7.4
			120	1267.3	965.0	1180.8	7.2	10.6	8.4
			180	897.4	836.1	981.4	11.0	13.1	10.9
		PEF	60	951.4	698.0	898.9	11.6	13.2	10.8
			120	620.6	699.9	751.0	18.7	13.9	13.5
			180	789.6	751.7	662.4	15.8	14.4	16.1
Sunset Yellow FCF	Pt	EF	60	222.7	266.8	3694.2	34.8	27.6	2.0
			120	463.4	446.2	636.3	17.6	16.8	12.6
			180	690.1	713.7	791.1	12.6	11.2	10.8
			240	921.2	1012.5	951.0	10.1	8.6	9.6
		PEF	60	235.1	256.3	4309.3	32.2	29.6	1.8
			120	343.4	416.1	652.9	23.1	19.3	12.6
			180	532.7	564.4	740.7	15.8	15.1	11.9
			240	749.2	742.4	870.4	12.4	12.5	11.0
	BDD	EF	60	580.5	591.8	429.6	15.6	15.1	20.1
			120	873.9	740.8	559.2	11.2	12.7	16.6
			180	1155.8	675.5	869.6	9.1	15.2	11.5
			240	1461.7	859.0	888.2	7.7	13.2	12.5
		PEF	60	425.5	511.2	295.4	20.7	17.3	30.1
			120	818.7	426.1	520.7	11.9	22.5	18.1
			180	1035.9	658.5	549.6	9.9	16.4	18.2
			240	1466.1	884.9	783.1	7.8	13.5	14.4

EC: energy consumption; TOC: total organic carbon; MCE: mineralization current efficiency; EF: electron-Fenton; PEF: photoelectron-Fenton; BDD: boron-doped diamond.

Fe^{2+}, presented lower EC and higher MCE. This is desirable because it enables the incineration of this compound under more environmentally friendly conditions, including a lower Fe^{2+} ion content. It seems that higher Fe^{2+} content interfered negatively with the performance of BDD. In this case, the excess Fe^{2+} may have favored the residual reaction (equation 19),[46] which can reduce the oxidation power of the process due to the consumption of hydroxyl radicals and the inhibition of the production of hydroxyl radicals by the Fenton reaction (equation 3).[46]

The trials of cathode $WO_{2.72}$ / Vulcan XC72 combined with the BDD anode showed the highest TOC removals: 82% TOC removal of OII by PEF / 1.00 after 3 h and 90% TOC removal of SY by PEF / 0.50 after 4 h. The results of mineralization also indicate that the electrochemical system (cathode: $WO_{2.72}$ / Vulcan XC72 and anode: BDD) employed in these experiments can become a good choice for dye removal. Both EF and FEP processes show superior or equal efficiency when compared to many other published studies, as shown in Table 5.

$$Fe^{2+} + {}^{\bullet}OH \rightarrow Fe^{3+} + OH^- \qquad (19)$$

Table 5. Comparative EF and PEF treatments of OII and SY dyes with GDE cathodes

Material	Process	Dye: C_0 / (mg C L^{-1}) (V_0 / mL)	TOC removal / % (time / h[a])	Reference
CNTF@CF	EF	OII: 19.2 (200)	28 (4)	[47]
PPy / lig-GF	EF	OII: 5.5 (200)	60 (3)	[36]
Air-diffusion cathode-BDD	PEF	SY: 100 (100)	95 (4)	[8]
$WO_{2.72}$ / Vn-BDD	EF	OII	72 (3)	this work[b]
$WO_{2.72}$ / Vn-BDD	PEF	OII	82 (3)	this work[b]
$WO_{2.72}$ / Vn-BDD	EF	SY	83 (4)	this work[b]
$WO_{2.72}$ / Vn-BDD	PEF	SY	90 (4)	this work[b]

[a]Electrolysis period; [b]C_0 = 50 mg C L^{-1} and V_0 = 350 mL. C_0: total organic carbon (TOC) initial concentration of dye; V_0: initial volume of solution; CNTF@CF: carbon nanotube fiber deposited on carbon fiber; EF: electro-Fenton; OII: Orange II; lig-GF: lig-GF: lignin-graphite felt; BDD: boron-doped diamond; PEF: photoelectro-Fenton; SY: Sunset Yellow FCF; Vn: Vulcan XC72.

Conclusions

Modification of Vulcan XC72 carbon by incorporating $WO_{2.72}$ nanoparticles resulted in increased H_2O_2 electrogeneration. The faster decolorization of SY can be attributed to its structure. Decolorizations with Pt anode were faster. However, mineralization with BBD anode showed higher yield. The Fe^{2+} initial concentration was determinant: 1.0 and 0.5 mmol L^{-1} Fe^{2+} were the most adequate concentrations for decolorization with Pt anode and mineralization with BDD anode, respectively. Thus, depending on the purpose, one should choose the most suitable anode to match it with the $WO_{2.72}$ / Vulcan XC72 cathode. The study showed the limitation of Pt anode to mineralize the studied dyes and allowed to identify the best parameters for application of the cathode of $WO_{2.72}$ / Vulcan XC72 at the combustion of OII and SY. The PEF process at 0.5 mol L^{-1} Fe^{2+} with BDD anode was shown to be more promising because it presented greater TOC removal and indicated a tendency of complete mineralization of the dyes. In addition, the study opens up possibilities to evaluate other parameters in order to obtain greater efficiency of the degradation process of dyes, considering that the cathode presented significant H_2O_2 electrogeneration.

Supplementary Information

Supplementary data are available free of charge at http://jbcs.sbq.org.br as PDF file.

Acknowledgments

References

1. Thiam, A.; Sirés, I.; Brillas, E.; *Water Res.* **2015**, *81*, 178.

2. Riaz, N.; Chong, F. K.; Man, Z. B.; Sarwar, R.; Farooq, U.; Khan, A.; Khan, M. S.; *RSC Adv.* **2016**, *6*, 55650.

3. Luo, F.; Yang, D.; Chen, Z.; Megharaj, M.; Naidu, R.; *J. Hazard. Mater.* **2016**, *303*, 145.

4. Roosta, M.; Ghaedi, M.; Sahraei, R.; Purkait, M. K.; *Mater. Sci. Eng., C* **2015**, *52*, 82.

5. Ghoneim, M. M.; El-Desoky, H. S.; Zidan, N. M.; *Desalination* **2011**, *274*, 22.

6. Brillas, E.; Garcia-Segura, S.; *Water Conserv. Sci. Eng.* **2016**, *1*, 83.

7. Ruiz, E. J.; Hernández-Ramírez, A.; Peralta-Hernández, J. M.; Arias, C.; Brillas, E.; *Chem. Eng. J.* **2011**, *171*, 385.

8. Moreira, F. C.; Garcia-Segura, S.; Vilar, V. J. P.; Boaventura, R. R.; Brillas, E.; *Appl. Catal., B* **2013**, *142-143*, 877.

9. Rache, M. L.; García, A. R.; Zea, H. R.; Silva, A. M. T.; Madeira, L. M.; Ramírez, J. H.; *Appl. Catal., B* **2014**, *146*, 192.

10. Nazar, M. F.; Murtaza, S.; *Color. Technol.* **2014**, *130*, 191.

11. Ramazanova, G. R.; Tikhomirova, T. I.; Apyari, V. V.; *J. Anal. Chem.* **2015**, *70*, 685.

12. Zazou, H.; Oturan, N.; Sonmez-Celebi, M.; Hamdani, M.; Oturan, M. A.; *J. Electroanal. Chem.* **2016**, *774*, 22.

13. Shin, Y. U.; Yoo, H. Y.; Kim, S.; Chung, K. M.; Park, Y. G.; Hwang, K. H.; Hong, S. W.; Park, H.; Cho, K.; Lee, J.; *Environ. Sci. Technol.* **2017**, *51*, 10700.

14. Sopaj, F.; Rodrigo, M. A.; Oturan, N.; Podvorica, F. I.; Pinson, J.; Oturan, M. A.; *Chem. Eng. J.* **2015**, *262*, 286.

15. Nidheesh, P. V; Zhou, M.; Oturan, M. A.; *Chemosphere* **2018**, *197*, 210.

16. Zhao, H.; Qian, L.; Guan, X.; Wu, D.; Zhao, G.; *Environ. Sci. Technol.* **2016**, *50*, 5225.

17. Aveiro, L. R.; da Silva, A. G. M.; Antonin, V. S.; Candido, E. G.; Parreira, L. S.; Geonmonond, R. S.; de Freitas, I. C.; Lanza, M. R. V.; Camargo, P. H. C.; Santos, M. C.; *Electrochim. Acta* **2018**, *268*, 101.

18. Carneiro, J. F.; Trevelin, L. C.; Lima, A. S.; Meloni, G. N.; Bertotti, M.; Hammer, P.; Bertazzoli, R.; Lanza, M. R. V.; *Electrocatalysis* **2017**, *8*, 189.

19. Moreira, F. C.; Boaventura, R. A. R.; Brillas, E.; Vilar, V. J. P.; *Appl. Catal., B* **2017**, *202*, 217.

20. Salazar, C.; Ridruejo, C.; Brillas, E.; Yánez, J.; Mansilla, H. D.; Sirés, I.; *Appl. Catal., B* **2017**, *203*, 189.

21. Yu, F.; Zhou, M.; Yu, X.; *Electrochim. Acta* **2015**, *163*, 182.

22. Garcia-Segura, S.; Brillas, E.; *Appl. Catal., B* **2016**, *181*, 681.

23. Moreira, F. C.; Garcia-Segura, S.; Boaventura, R. A. R.; Brillas, E.; Vilar, V. J. P.; *Appl. Catal., B* **2014**, *160-161*, 492.

24. Faust, B. C.; Zepp, R. G.; *Environ. Sci. Technol.* **1993**, *27*, 2517.

25. Paz, E. C.; Aveiro, L. R.; Pinheiro, V. S.; Souza, F. M.; Lima, V. B.; Silva, F. L.; Hammer, P.; Lanza, M. R. V.; Santos, M. C.; *Appl. Catal., B* **2018**, *232*, 436.

26. Assumpção, M. H. M. T.; De Souza, R. F. B.; Reis, R. M.; Rocha, R. S.; Steter, J. R.; Hammer, P.; Gaubeur, I.; Calegaro, M. L.; Lanza, M. R. V.; Santos, M. C.; *Appl. Catal., B* **2013**, *142-143*, 479.

27. Assumpção, M. H. M. T.; Moraes, A.; De Souza, R. F. B.; Gaubeur, I.; Oliveira, R. T. S.; Antonin, V. S.; Malpass, G. R. P.; Rocha, R. S.; Calegaro, M. L.; Lanza, M. R. V.; Santos, M. C.; *Appl. Catal., A* **2012**, *411-412*, 1.

28. Forti, J. C.; Rocha, R. S.; Lanza, M. R. V.; Bertazzoli, R.; *J. Electroanal. Chem.* **2007**, *601*, 63.

29. Carneiro, J. F.; Rocha, R. S.; Hammer, P.; Bertazzoli, R.; Lanza, M. R. V.; *Appl. Catal., A* **2016**, *517*, 161.

30. *CasaXPS Processing Software*; Casa Software Ltd., Teignmouth, UK, http://www.casaxps.com.

31. Shukla, S.; Chaudhary, S.; Umar, A.; Chaudhary, G. R.; Kansal, S. K.; Mehta, S. K.; *Chem. Eng. J.* **2016**, *288*, 423.

32. Antonin, V. S.; Parreira, L. S.; Aveiro, L. R.; Silva, F. L.; Valim, R. B.; Hammer, P.; Lanza, M. R. V; Santos, M. C.; *Electrochim. Acta* **2017**, *231*, 713.

33. Wang, Y.; Liu, Y.; Wang, K.; Song, S.; Tsiakaras, P.; Liu, H.; *Appl. Catal., B* **2015**, *165*, 360.

34. Barros, W. R. P.; Reis, R. M.; Rocha, R. S.; Lanza, M. R. V.; *Electrochim. Acta* **2013**, *104*, 12.

35. Xia, G.; Lu, Y.; Xu, H.; *Electrochim. Acta* **2015**, *158*, 390.

36. Huang, H.; Han, C.; Wang, G.; Feng, C.; *Electrochim. Acta* **2018**, *259*, 637.

37. Liang, L.; Yu, F.; An, Y.; Liu, M.; Zhou, M.; *Environ. Sci. Pollut. Res.* **2017**, *24*, 1122.

38. Tang, Q.; Wang, D.; Yao, D. M.; Yang, C. W.; Sun, Y. C.; *Water Sci. Technol.* **2016**, *73*, 1652.

39. Sirés, I.; Garrido, J. A.; Rodríguez, R. M.; Brillas, E.; Oturan, N.; Oturan, M. A.; *Appl. Catal., B* **2007**, *72*, 382.

40. Dai, H.; Xu, S.; Chen, J.; Miao, X.; Zhu, J.; *Chemosphere* **2018**, *199*, 147.

41. Pereira, G. F.; El-Ghenymy, A.; Thiam, A.; Carlesi, C.; Eguiluz, K. I. B.; Salazar-Banda, G. R.; Brillas, E.; *Sep. Purif. Technol.* **2016**, *160*, 145.

42. Antonin, V. S.; Garcia-Segura, S.; Santos, M. C.; Brillas, E.; *J. Electroanal. Chem.* **2015**, *747*, 1.

43. Thiam, A.; Brillas, E.; Garrido, J. A.; Rodríguez, R. M.; Sirés, I.; *Appl. Catal., B* **2016**, *180*, 227.

44. Thiam, A.; Sirés, I.; Garrido, J. A.; Rodríguez, R. M.; Brillas, E.; *J. Hazard. Mater.* **2015**, *290*, 34.

45. Jalife-Jacobo, H.; Feria-Reyes, R.; Serrano-Torres, O.; Gutiérrez-Granados, S.; Peralta-Hernández, J. M.; *J. Hazard. Mater.* **2016**, *319*, 78.

46. Lin, H.; Zhang, H.; Wang, X.; Wang, L.; Wu, J.; *Sep. Purif. Technol.* **2014**, *122*, 533.

47. Le, T. X. H.; Alemán, B.; Vilatela, J. J.; Bechelany, M.; Cretin, M.; *Front. Mater.* **2018**, *5*, 9.